EXPERIMENTALLY AND NUMERICALLY INVESTIGATED FILM COOLING IN A SUBSCALE ROCKET COMBUSTION CHAMBER

*R. Arnold**, D. I. Suslov*, M. Oschwald* and O. J. Haidn**
*T. Aichner**, B. Ivancic** and M. Frey***

** German Aerospace Center (DLR), Institute of Space Propulsion, Lampoldshausen*
74239 Hardthausen, Germany
*** Astrium GmbH, Space Transportation, Launcher Propulsion*
81663 Munich, Germany

Abstract—Film cooling is a widely-used cooling technique to reduce the hot gas side wall temperatures in turbines and combustors of airbreathing engines as well as in rocket thrust chambers. Prepared in the framework of the German National Technology Programme on Cryogenic Rocket Engines (TEKAN II), the paper presents the comparison of experimental film cooling data and heat flux results with numerical simulations. The experiments have been performed at the European Research and Technology Test Facility P8 at DLR Lampoldshausen, whereas the simulations have been carried out at Astrium GmbH, Munich, applying the spray combustion code Rocflam-II. Experimental data and numerical simulations show good agreement within the investigated range of chamber pressures and film cooling mass flow rates.

1. INTRODUCTION

ROCKET engines are one of the most powerful machines ever developed, featuring a thermal power of several gigawatts. To provide the enormous high power density inside a combustion chamber of a typical rocket engine, high energetic and cryogenic propellants like liquid oxygen (LOX) and liquid hydrogen (LH_2) are used. Herewith, hot gas temperatures $T_{cc} > 3500\,K$ arise with combustion chamber pressures p_{cc} exceeding 10 MPa by far (SSME: p_{cc} = 19 MPa [1]; RD-0120: p_{cc} = 21.8 MPa [2]). Due to hot gas temperatures and combustion chamber pressures, local wall heat flux densities q of more than $100\,MW/m^2$ have to be compensated by the cooling system of the engine. Especially the throat area with maximum wall heat flux densities, as pictured in Figure 1 (a) for a typical first stage engine operated with LOX/H_2 (calculated with the Two-Dimensional Kinetics TDK 91/PRO Nozzle Performance Computer Program [3]) needs precise and extensive cooling efforts to survive during hot run. A typical example for a LOX/LH_2 first stage rocket engine is the Vulcain 2 of the European launcher Ariane 5, shown in Figure 1 (b) during a hot run on the P5 test bench at DLR Lampoldshausen.

A major design criterion for future reusable high pressure rocket engines is a considerable improvement of reliability and overall system efficiency at low cost. The achievement of these ambitious goals demands further developments of current combustion chamber technology, which means for example a combination of several different cooling techniques like regenerative and film cooling in concurrence with new high temperature materials. One of the limiting factors in

*Corresponding author; currently Post Doctoral Scientist at Purdue University, School of Aeronautics and Astronautics, Maurice J. Zucrow Laboratories, 500 Allison Road, West Lafayette, IN 47907, USA.

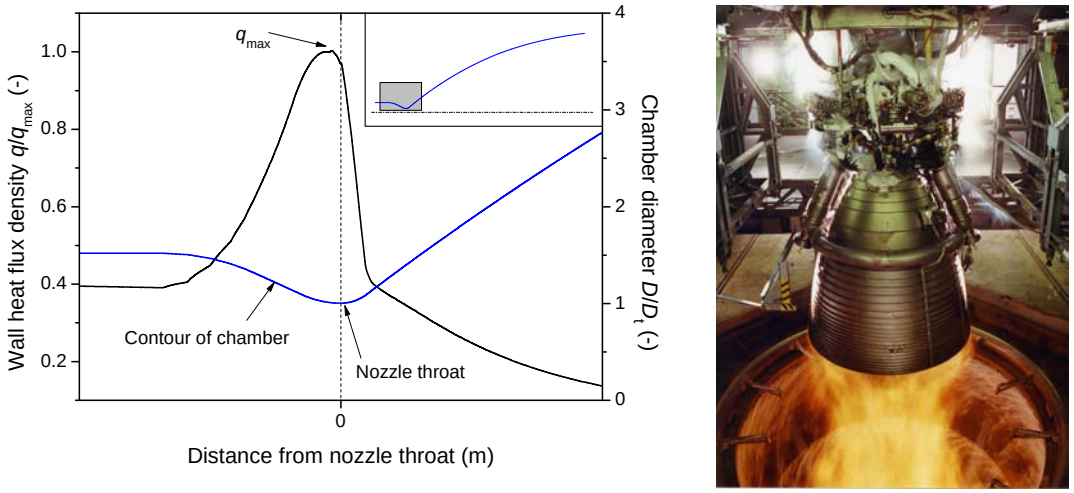

(a) Heat flux distribution (TDK 91/PRO [3] calculation)

(b) Vulcain 2 engine [4]

Figure 1: Typical wall heat flux distribution and Vulcain 2 engine

designing reusable next generation high pressure rocket engines is the limited knowledge and understanding of combustion processes. Hot gas side heat transfer and cooling efficiency on the one hand, and heavily loaded fuel turbopumps and turbines because of the high pressure drop of mainly regenerative cooled systems on the other hand, which results in a reduced life time of the turbomachinery and hence the whole system. Future high pressure rocket engines which allow extended reusability may therefore use film cooling in combination with regenerative cooling even more intensely than up-to-date film cooled engines like Vulcain 2, SSME and RD-170. However, there is a general necessity to investigate film cooling behavior in subscale combustion chambers under real rocket engine like conditions. The understanding of these phenomena may lead directly to future applications with very high combustion chamber pressure and engine performance with only a limited performance reduction due to film cooling, and can also help to validate numerical tools for the design of even more effectively cooled chambers.

In the past, a variety of different cooling systems for short and long duration applications have been developed to guarantee a safe and steady-state temperature distribution inside the chamber wall material during hot-run [5]:

- Ablative cooling is used especially for short-duration systems like booster engines with a limited operating time of about 2 minutes.
- Radiation cooling. With this method, comparatively low heat flux areas of liquid rocket engines like nozzle extensions are cooled.
- Dump cooling. With this principle, the coolant is pouring through cooling channels inside the liner material and is dumped overboard at the end of the nozzle skirt through sonic outlets.
- Regenerative cooling. Like dump cooling, the coolant flows through cooling channels, but afterwards is injected into the combustion chamber.
- Film cooling. This method can be used either alone for low heat flux areas or in combination with regenerative cooling for very high heat flux densities.

2. Experimental Setup and Operational Conditions

A short overview of the subscale combustion chamber and the operating conditions performed at the European Research and Technology Test Facility P8 will be presented in the following sec-

tions. A more detailed description of the hardware, measurement technique, instrumentation and the operating conditions can be found in previous DLR publications with regard to film cooling investigations using subscale combustion chamber "E" [6, 7, 8].

2.1 Subscale combustion chamber "E"

The cylindrical segment of subscale combustion chamber "E", depicted in Figure 3 (a) features an overall length of 200 mm and an inner diameter of 50 mm. Convective cooling of the segment is provided by water which is heated when flowing through cooling channels. Like the cylindrical segment, the nozzle throat segment is also cooled by water. The throat diameter in the nozzle segment is 33 mm.

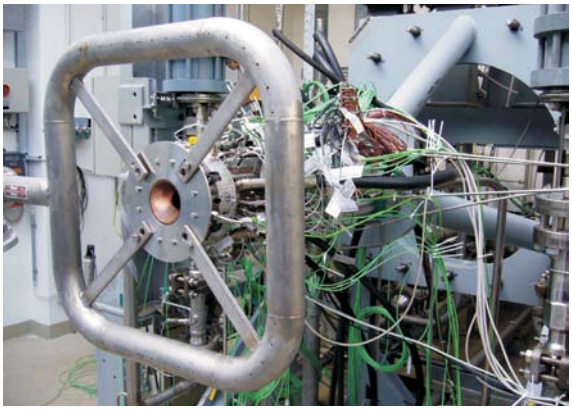

Figure 2: Combustion chamber "E" at P8

Figure 2 depicts subscale combustion chamber "E" attached at the test facility P8. The coaxial injector head is built up with 15 individual injection elements, arranged at two different pitch circles with ten coaxial injector elements at the outer circle and five at the inner circle. The geometrical distribution of the injector elements is made in the way to get five identical injector triangles (see Figure 3 (b)).

For film cooling investigations, the injector head face plate is surrounded by a coolant injection segment. This segment provides ten evenly distributed, in circumferential direction arranged cooling slots for tangential film coolant injection. Positions of these film cooling slots are consistent with the angular positions of the coaxial injector elements from the outer injector head pitch circle. Inside one of the injector triangles, film coolant injection slots and outer coaxial injector elements are located at the angular positions $\xi = 0°$ and $\xi = 36°$, whereas the position of the inner coaxial injector element is $\xi = 18°$ (see Figure 3 (b)). The coolant injection slots feature a slot height of 0.4 mm and a slot width of 3.5 mm.

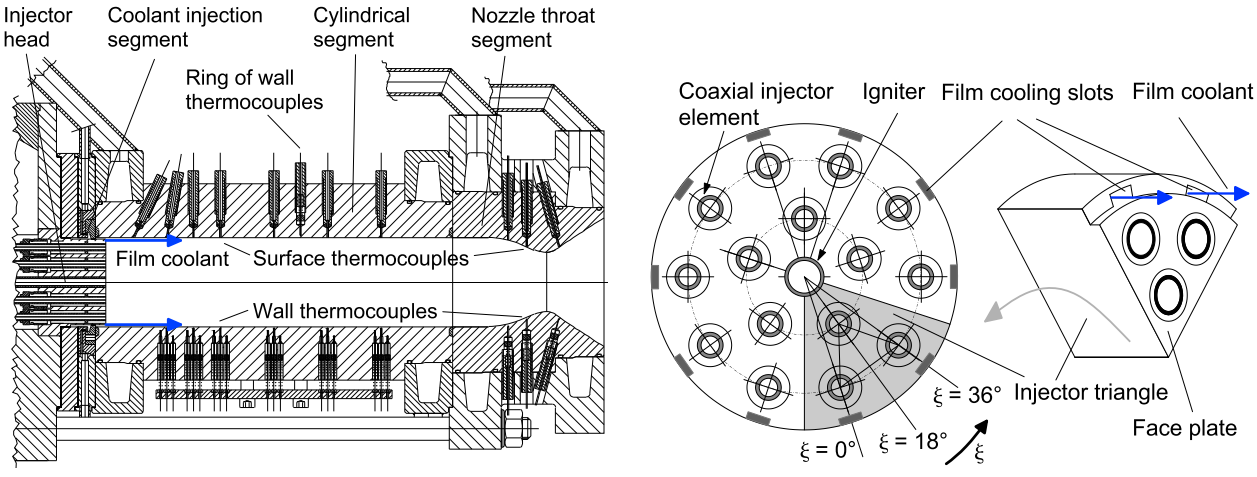

(a) Subscale combustion chamber "E"

(b) Injector head and film injection segment

Figure 3: Experimental setup

For the detection of surface temperatures inside the combustion chamber, packages each with three wall thermocouples at different wall distances were implemented for the measurement of the thermal gradient inside the chamber wall material positioned almost perpendicular to the chamber

surface (*gradient method*). Surface thermocouples were used for the direct detection of the hot gas side wall temperature (see Figure 3 (a)). The measurement of the wall heat flux density has been done firstly by measuring the enthalpy change of the coolant water (*caloric method*), which is a relatively simple and reliable method for detecting the wall heat flux density, though only averaged heat fluxes can be measured. Secondly, the gradient method, which allows also local detection of the wall heat flux density was applied as the preferred method for the present investigations [9].

2.2 Operating conditions

Three major pressure levels have been performed with subscale combustion chamber "E": 11.5 MPa (intervals 1...3), 8 MPa (intervals 4...6) and 5 MPa (intervals 7...9), using a constant propellant mixture ratio $ROF = 6$. However, for the numerical simulations described in the present paper only the 11.5 MPa (Vulcain 2 like condition) and 8 MPa pressure levels have been taken into account (see Figure 4 (a)).

During each hot run, the pressure levels have been divided into intervals with different film coolant mass flow rates: in terms of the total fuel and oxidizer mass flow rate, approximately 2 %, approximately 1 %, and for the last section 0 % have been performed. However, in terms of the total fuel mass flow rate – given by the fuel and the film cooling $\dot{m}_2/(\dot{m}_{\text{fuel}} + \dot{m}_2)$ – film cooling mass flow rates of approximately 12 % for the first interval and approximately 6.5 % for the second interval have been used (see Figure 4 (b)). Gaseous hydrogen (GH_2) with ambient temperature has been injected for all tests as film coolant [6, 10, 11].

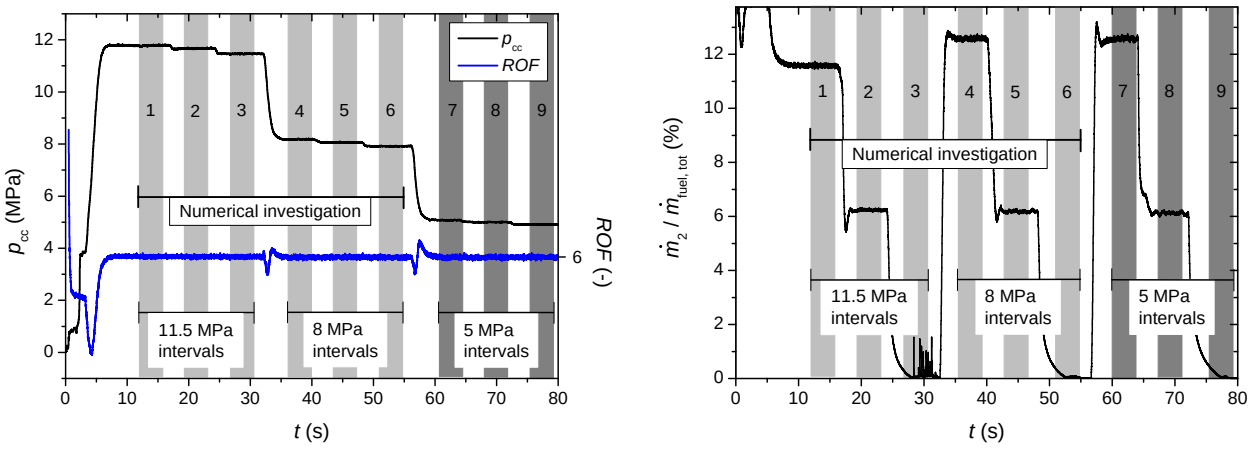

(a) Combustion chamber pressure and mixture ratio

(b) Film coolant mass flow rate

Figure 4: Pressure, mixture ratio and film mass flow rates

Table 1 summarizes hot gas parameters like chamber pressure p_{cc} and propellant mixture ratio ROF as well as film coolant parameters like film injection temperature T_2 and film mass flow rates in relation to the total injector mass flow rates $\dot{m}_{tot}$ and the total fuel mass flow rates $\dot{m}_2/\dot{m}_{fuel,tot}$.

Table 1: Operating conditions

	Interval 1	**Interval 2**	**Interval 3**	**Interval 4**	**Interval 5**	**Interval 6**
p_{cc} (MPa)	11.9	11.8	11.6	8.3	8.2	8.0
ROF (-)	6.02	6.00	5.99	5.99	5.99	5.99
$\dot{m}_2/\dot{m}_{tot}$ (%)	1.83	1.03	0	2.01	0.99	0
$\dot{m}_2/\dot{m}_{fuel,tot}$ (%)	11.4	6.7	0	12.3	6.5	0
T_2 (K)	287.5	287.5	–	288.3	289.2	–

3. Instrumentation and measurement technique

For the measurement of film cooling effectiveness and local wall heat flux density subscale combustion chamber "E" is equipped with wall thermocouples, which are arranged in packages of three with different wall distances $d_1 \dots d_3$ from the hot gas side [6, 10, 11]. By measuring the thermal gradient inside the chamber wall material it is possible to extrapolate the surface temperature ($d = 0$) with the use of Fourier's law of heat conduction for constant properties [12]:

$$\underbrace{\frac{\partial T}{\partial t}}_{0} = a\left(\frac{\partial^2 T}{\partial x^2} + \underbrace{\frac{\partial^2 T}{\partial y^2}}_{0} + \underbrace{\frac{\partial^2 T}{\partial z^2}}_{0}\right) + \underbrace{\frac{\dot{q}_i}{\rho c}}_{0} \tag{1}$$

With the assumption of a rotation-symmetrically constructed chamber geometry (radius r), the logarithmic temperature distribution perpendicular to the hot gas side surface inside the chamber wall material can be written as a function of the wall distance h (*gradient method*):

$$\begin{aligned} \frac{\partial^2 T}{\partial (r+h)^2} + \frac{1}{r+h}\frac{\partial T}{\partial (r+h)} &= 0 \\ \rightarrow T(r+h) &= T_{\mathrm{W1}} + \frac{T_{\mathrm{W2}} - T_{\mathrm{W1}}}{\ln\left(\frac{r+h_2}{r+h_1}\right)} \ln\left(\frac{r+h}{r+h_1}\right) \end{aligned} \tag{2}$$

By using the logarithmic temperature distribution following equation (2), the local wall heat flux density can be calculated as ($\lambda_{\text{Elbrodur® G}} = 350\,\mathrm{W/(mK)}$ [13]):

$$q = \frac{\lambda}{r}\frac{T_{\mathrm{W1}} - T_{\mathrm{W2}}}{\ln\left(\frac{r+h_2}{r+h_1}\right)} \tag{3}$$

Experimental results in terms of surface temperature and wall heat flux density–equations (2) and (3) respectively–have provided the data base for the comparison with numerical simulations discussed in the present paper.

4. Numerical simulations

Numerical simulations of subscale combustion chamber "E" have been performed at Astrium GmbH, Munich, using coupled numerical simulations of hot gas and coolant side (conjugate heat transfer). For the hot gas side, the in-house spray combustion code Rocflam-II [14, 15] has been applied. Rocflam-II combines a Lagrangian tracking module treating the injection, atomization and evaporation of propellants with a Navier-Stokes-solver, where the flow including mixing, chemical reactions and the expansion in the divergent part is computed.

Different propellant injection possibilities are offered by Rocflam-II, depending on the thermodynamic state of the fluid. For two gaseous components, the Lagrangian droplet tracking module can be switched off, and the propellants can be injected through openings in the wall. Alternatively, the gaseous components can be injected as source terms in the conservation equations for mass, momentum, enthalpy and concentration or mixture fraction, i. e. a wall opening is not necessary. For liquid rocket engines, however, the propellants are injected in liquid or supercritical state. For the load points applied to combustion chamber "E", the fuel H_2 is injected at a pressure of about 8 MPa and about 11.5 MPa, respectively, and at temperatures around 290 K. Compared to the critical point ($p_{\mathrm{crit}} = 1.284$ MPa, $T_{\mathrm{crit}} = 32.94$ K [16]), this is far overcritical in both pressure and temperature, and the fluid behavior is comparable to a gas. The oxidizer O_2 is injected at the same pressure (8 MPa and 11.5 MPa, respectively) and at a lower temperature of only about 110 K.

Again comparing to the critical state (p_{crit} = 5.043 MPa, T_{crit} = 154.58 K [16]), this is overcritical in pressure, but undercritical in temperature. In terms of compressibility, the behaviour of the oxidizer is more liquid like, although there is no more surface tension and phase change possible. For such injection circumstances, the best practice in Rocflam-II is to inject the oxidizer as droplet in the Lagrangian droplet tracking module, while the fuel is injected as a gaseous source term directly into the Navier-Stokes solver. Also the injected film in combustion chamber "E" is injected via gaseous source terms. Hence, no openings in the face plate are necessary.

Rocflam-II includes two different chemistry models, both taking into account turbulent combustion: First, a global chemistry based on globally defined reactions is available, where the reaction rate is determined with an eddy-dissipation concept formulation. For each species concentration, a dedicated differential equation is solved. Second, there is an equilibrium table-based chemistry model with a one-dimensional presumed probability density function (ppdf) approach taking into account the influence of turbulent combustion. No species concentration equations are solved, only a global mixture fraction and its variance are treated by differential equations. For the chemistry of H_2/O_2 combustion the ppdf approach is used.

The cooling channels of the chamber are simulated with the commercial flow solver ANSYS CFX 11. One cooling channel is resolved in detail (3D) with 800000 nodes. The simulation is of 2nd order (high resolution) and the turbulence model used for the cooling side is SST (shear stress transport) with automatic wall functions. The material of the wall is a CuCrZr alloy (Elbrodur® G) which was simulated with proper material data. The outer walls are modelled as adiabatic, side walls have a symmetry condition and the hot combustor wall is the interface to the Rocflam-II side. Here the heat flux is taken into account by averaging the temperature in circumferential direction for each axial position to generate the transfer data for the 2D-hot gas side.

Rocflam-II and CFX are loosely coupled, with the Rocflam-II wall heat flux used as boundary condition for the coolant side simulation, while CFX wall temperatures are the boundary condition for the hot gas side simulation. After several coupling iterations, as convergence is reached, wall temperature and wall heat flux can be determined in this way.

5. Experimental and numerical results

Simulations for six different load points of chamber E have been carried out: Two load points without film cooling and a combustion chamber pressure p_{cc} = 8 MPa and p_{cc} = 11.5 MPa respectively, and two load points for each of these pressure levels with a film rate of about 6.5 % and of about 12 % (see Figure 4). The main results the coupled Rocflam-II CFX simulations provide are temperature distribution and gas composition inside the combustion chamber, the combustion efficiency and, as an important contribution to combustion chamber design, values at the wall, as wall heat flux and wall temperature. At the coolant side the simulation provides design parameters as the local temperature of the cooling fluid and the pressure drop inside the cooling channel. A typical temperature and mixture ratio distribution in the combustion chamber "E" is shown in Figure 5.

Figure 5 (a) shows the distribution for the load point p_{cc} = 8 MPa without film whereas Figure 5 (b) shows the load point p_{cc} = 11.5 MPa without film. On the lower part of each figure the temperature distribution is displayed. In the area near the face-plate cold areas (blue) can be observed. Two hot streaks (yellow) indicate the two injection rows where the H_2 source terms and the O_2 droplets are initialised. Further downstream the propellants mix and combust. This can also be observed in the mixture ratio distribution in the upper part of the figure where blue regions show fuel rich regions which are almost totally filled with H_2. The red streaks near the face plate show oxidizer rich regions which indicate the O_2 injection jet. The thin yellow-green streaks in between mark the shear layer between the two propellants which start to mix in these regions and react. Further downstream the high gradients in mixture ratio are reduced and the green colour further downstream, close to the convergent part of the combustion chamber, indicates a mixture ratio

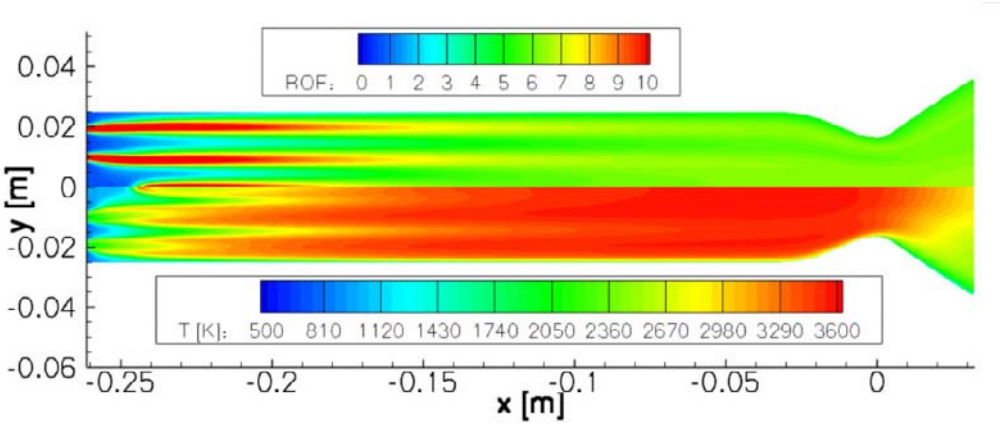

(a) Load point 8 MPa without film

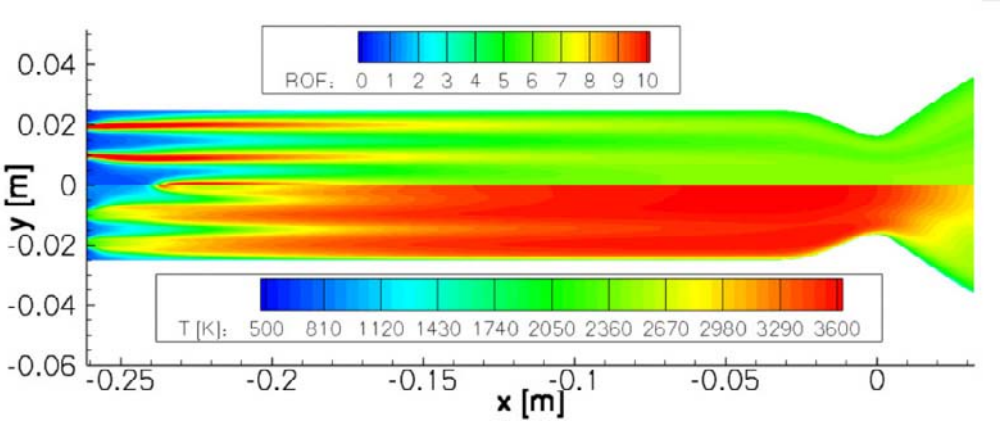

(b) Load point 11.5 MPa without film

Figure 5: Typical temperature distribution (bottom of each figure) and mixture ratio distribution (top of each figure) for a simulation of chamber "E", coupled Rocflam-II/CFX simulation

close to the injected mixture ratio $ROF = 6$. The remaining level of stratification of the mixture ratio in the throat cross section is an indicator for the combustion efficiency reached in the combustion chamber. The combustion efficiency is also an important design parameter which is evaluated with Rocflam-II and will be discussed below.

In Figure 6 several axial cuts of one cooling channel of the cylindrical segment (see Figure 3 (a)) are displayed. The heating along the length of the combustor is clearly visible.

In Figure 7 the simulated wall temperature and wall heat flux are compared to the measurement. The figures show the load points $p_{cc} = 8$ MPa without film (Figure 7 (a)), $p_{cc} = 11.5$ MPa without film (Figure 7 (c)), $p_{cc} = 8$ MPa, 12 % film rate (Figure 7 (b)) and $p_{cc} = 11.5$ MPa, 12 % film rate (Figure 7 (d)). All four simulations show good overall agreement for these four load points. The level of the wall temperature and wall heat flux is determined well, although the increase of the temperature along x seems to be somewhat steeper in the measured data. The application of 12 % film rate decreases the wall temperature roughly about 80 K as well for the 8 MPa load points as for the 11.5 MPa load points.

η_{c^*} characterizes the quality of combustion by comparing the actually measured or simulated characteristic velocity c^* to its theoretical 1D value. The characteristic velocity can be described as a function of the chamber pressure p_{cc}, throat diameter A_t and mass flow rate $\dot{m}$:

$$c^* = \frac{p_{cc} A_t}{\dot{m}} \tag{4}$$

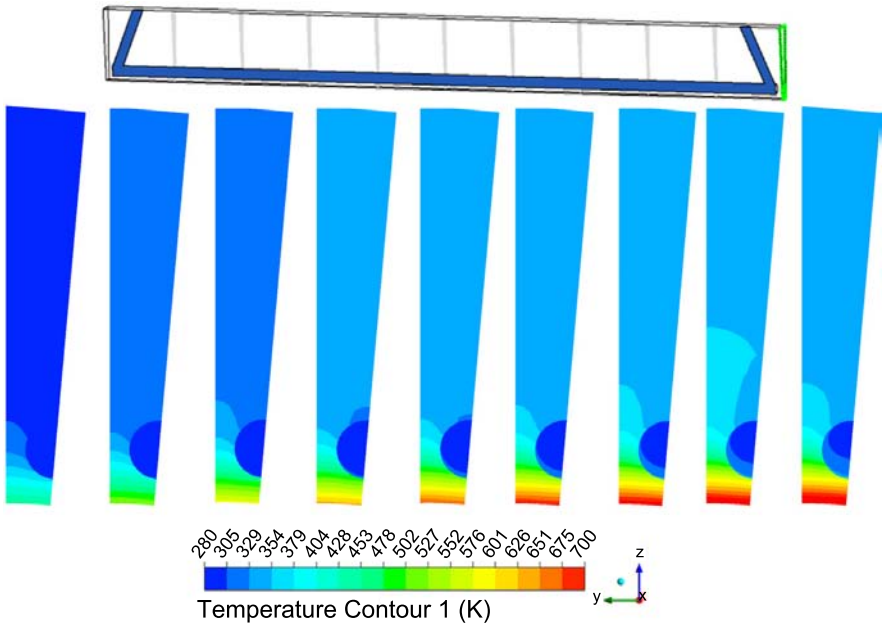

Figure 6: Different axial cuts of the simulated cooling channel, coupled Rocflam-II/CFX simulation (11.5 MPa, 6.7% film mass flow rate)

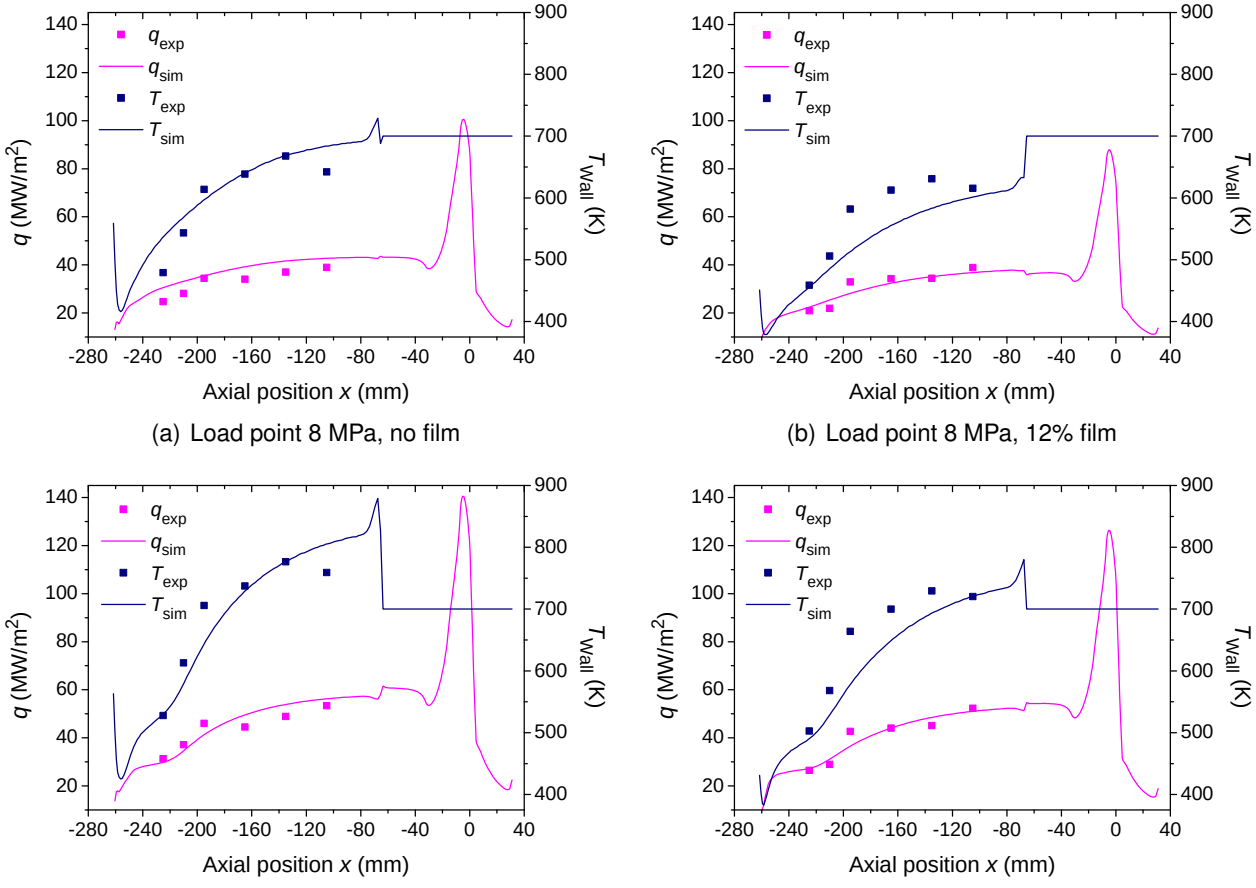

(a) Load point 8 MPa, no film

(b) Load point 8 MPa, 12% film

(c) Load point 11.5 MPa, no film

(d) Load point 11.5 MPa, 12% film

Figure 7: Comparison of simulated (Rocflam-II/CFX) wall temperature and wall heat flux density with experimental data

The combustion efficiency η_{c^*} is given by:

$$\eta_{c^*} = \frac{c^*}{c^*_{theoretical}} \tag{5}$$

Regarding to the combustion efficiency η_{c^*}, an increase of the film mass flow rate up to 12 % leads to a decrease in efficiency of approx. 1.1 % (8 MPa) and approx. 0.6 % (11.5 MPa), respectively (see Table 2). This effect can be explained by increased mixture ratio stratification in the throat cross section with an increased film mass flow rate due to incomplete mixture of the film with the core flow.

Table 2: η_{c^*} values resulting from coupled Rocflam-II/CFX simulation

	Interval 1	**Interval 2**	**Interval 3**	**Interval 4**	**Interval 5**	**Interval 6**
p_{cc} (MPa)	11.5	11.5	11.5	8.0	8.0	8.0
ROF_{core} (-)	6	6	6	6	6	6
ROF_{tot} (-)	5.3	5.6	6	5.2	5.6	6
film rate (%)	11.4	6.7	–	12.3	6.5	–
Rocflam-II:						
η_{c^*} (%)	97.1	97.7	97.7	96.5	97.3	97.6

6. CONCLUSIONS

For the present study, experimentally measured and numerically simulated data of a high pressure subscale combustion chamber have been compared within a cooperation of DLR, Lampoldshausen and Astrium, Munich. The comparison in terms of wall temperature distribution and heat flux density has shown a good agreement for the investigated chamber pressure levels 8 MPa and 11.5 MPa with and without film cooling. Also the influence of the film cooling on the combustion efficiency has been analyzed with a slight decrease of the efficiency due to the application of an injected film.

Further numerical investigations at Astrium will delve into the simulation of different film coolant mass flow rates for each pressure level. Furthermore, a new 2-dimensional inverse method for the recalculation of wall heat flux from the temperature measurements has been developed recently at DLR, showing promising results in comparison with the gradient method used so far.

ACKNOWLEDGEMENT

The Astrium part of the presented content was elaborated within the technology programme TEKAN 2010 II which is sponsored by the German National Space Agency DLR under contract 50RL0710.

REFERENCES

[1] G. P. Sutton. History of Liquid Propellant Rocket Engines in the United States. *Journal of Propulsion and Power*, Vol. 19, No. 6:978–1007, 2003.

[2] G. P. Sutton. History of Liquid-Propellant Rocket Engines in Russia, Formerly the Soviet Union. *Journal of Propulsion and Power*, Vol. 19, No. 6:1008–1037, 2003.

[3] S. S. Dunn, D. E. Coats, G. R. Nickerson, and D. R. Berker. *Two-Dimensional Kinetics (TDK 91/PRO) Nozzle Performance Computer Program*. Software & Engineering Associates, Inc., Carson City, NV, November 21th 1991.

[4] Deutsches Zentrum für Luft- und Raumfahrt e. V. (DLR), Institut für Raumfahrtantriebe. *http://www.dlr.de/ra/*. Lampoldshausen, 74239 Hardthausen, December 2007.

[5] D. K. Huzel and D. H. Huang. *Modern Engineering for Design of Liquid-Propellant Rocket Engines*, volume 147 of *Progress in Astronautics and Aeronautics*. American Institute of Aeronautics and Astronautics (AIAA), Rocketdyne Division of Rockwell International, ISBN 1-56347-013-6, 1992.

[6] R. Arnold. *Experimentelle Untersuchungen zur Filmkühlung in Raketenbrennkammern*. PhD thesis, Universität Stuttgart, December 2008.

[7] R. Arnold, D. Suslov, and O. J. Haidn. Circumferential Film Cooling Effectiveness in a LOX/H_2 Subscale Combustion Chamber. *Journal of Propulsion and Power*, Vol. 25, No. 3:760–770, May-June 2009.

[8] R. Arnold, D. Suslov, and O. J. Haidn. Film Cooling of Accelerated Flow in a Subscale Combustion Chamber. *Journal of Propulsion and Power*, Vol. 25, No. 2:443–451, March-April 2009.

[9] D. Suslov, A. Woschnak, J. Sender, and M. Oschwald. Test Specimen Design and Measurement Technique for Investigation of Heat Transfer Processes in Cooling Channels of Rocket Engines under Real Thermal Conditions. In *24th International Symposium on Space Technology and Science (ISTS)*, Miyazaki, Japan, May 30th-June 6th 2004. ISTS 2004-e-40.

[10] R. Arnold, D. Suslov, and O. J. Haidn. Influence Parameters on Film Cooling Effectiveness in a High Pressure Subscale Combustion Chamber. In *47th AIAA Aerospace Sciences Meeting*, Orlando, FL, January 4th-8th 2009. AIAA-2009-0453.

[11] R. Arnold, D. Suslov, B. Weigand, and O. J. Haidn. Circumferential Behavior of Tangential Film Cooling and Injector Wall Compatibility in a High Pressure LOX/GH_2 Subscale Combustion Chamber. In *44th AIAA/ASME/SAE/ASEE Joint Propulsion Conference and Exhibit*, Hartford, CT, July 21st-23rd 2008. AIAA-2008-5242.

[12] H. Büttner and Mokross. Fourier's Law and Thermal Conduction. *Nature*, Vol. 311:217–218, September 1984.

[13] M. Oschwald, D. Suslov, and A. Woschnak. Einfluss der Temperaturabhängigkeit der Materialeigenschaften auf den Wärmehaushalt in regenerativ gekühlten Brennkammern. In *Deutscher Luft- und Raumfahrtkongress*, Dresden, 20.-23. September 2004. DGLR-2004/111.

[14] J. Görgen, T. Aichner, and M. Frey. Spray Combustion and Heat Transfer Modelling in LOX/H_2, LOX/HC and MMH/NTO Combustion Chambers. In *3rd European Conference for Aero-Space Sciences (EUCASS)*, Paris, France, July 6th-9th 2009. EUCASS2009-104.

[15] M. Frey, B. Knieser, and O. Knab. Consideration of Real Gas Effects and Condensation in a Spray Combustion Rocket Thrust Chamber Design Tool. In *3rd European Conference for Aero-Space Sciences (EUCASS)*, Paris, France, July 6th-9th 2009. EUCASS2009-85.

[16] B. A. Younglove. Thermophysical Properties of Fluids. I. Argon, Ethylene, Parahydrogen, Nitrogen, Nitrogen Trifluoride, and Oxygen. *Journal of Physical and Chemical Reference Data*, Vol. 11, Supplement No. 1, 1982.